A model of radiation action based on nanodosimetry and the application to ultra-soft X-rays

Schneider, Uwe ; Vasi, Fabiano ; Schmidli, Kevin ; Besserer, Jürgen

Abstract: A radiation action model based on nanodosimetry is presented. It is motivated by the finding that the biological effects of various types of ionizing radiation lack a consistent relation with absorbed dose. It is postulated that the common fundamental cause of these effects is the production of elementary sublesions (DSB), which are created at a rate that is proportional to the probability to produce more than two ionisations within a volume of 10 base pairs of the DNA. The concepts of nanodosimetry allow for a quantitative characterization of this process in terms of the cumulative probability F2. The induced sublesions can interact in two ways to produce lethal damage. First, if two or more sublesions accumulate in a locally limited spherical volume of 3–10 nm in diameter, clustered DNA damage is produced. Second, consequent interactions or rearrangements of some of the initial damage over larger distances (µm) can produce additional lethal damage. From the comparison of theoretical predictions deduced from this concept with experimental data on relative biological effectiveness, a cluster volume with a diameter of 7.5 nm could be determined. It is shown that, for electrons, the predictions agree well with experimental data over a wide energy range. The only free parameter needed to model cell survival is the intersection cross-section which includes all relevant cell-specific factors. Using ultra-soft X-rays it could be shown that the energy dependence of cell survival is directly governed by the nanodosimetric characteristics of the radiation track structure. The cell survival model derived in this work exhibits exponential cell survival at a high dose and a finite gradient of cell survival at vanishing dose, as well as the dependence on dose-rate.

DOI: https://doi.org/10.1007/s00411-020-00842-1

Radiation and Environmental Biophysics (2020) 59:439–450
https://doi.org/10.1007/s00411-020-00842-1

ORIGINAL ARTICLE

A model of radiation action based on nanodosimetry and the application to ultra-soft X-rays

Uwe Schneider[1,2] · Fabiano Vasi[1,2] · Kevin Schmidli[1,2] · Jürgen Besserer[1,2]

Received: 28 November 2019 / Accepted: 30 March 2020 / Published online: 10 April 2020

Abstract
A radiation action model based on nanodosimetry is presented. It is motivated by the finding that the biological effects of various types of ionizing radiation lack a consistent relation with absorbed dose. It is postulated that the common fundamental cause of these effects is the production of elementary sublesions (DSB), which are created at a rate that is proportional to the probability to produce more than two ionisations within a volume of 10 base pairs of the DNA. The concepts of nanodosimetry allow for a quantitative characterization of this process in terms of the cumulative probability F_2. The induced sublesions can interact in two ways to produce lethal damage. First, if two or more sublesions accumulate in a locally limited spherical volume of 3–10 nm in diameter, clustered DNA damage is produced. Second, consequent interactions or rearrangements of some of the initial damage over larger distances (~ µm) can produce additional lethal damage. From the comparison of theoretical predictions deduced from this concept with experimental data on relative biological effectiveness, a cluster volume with a diameter of 7.5 nm could be determined. It is shown that, for electrons, the predictions agree well with experimental data over a wide energy range. The only free parameter needed to model cell survival is the intersection cross-section which includes all relevant cell-specific factors. Using ultra-soft X-rays it could be shown that the energy dependence of cell survival is directly governed by the nanodosimetric characteristics of the radiation track structure. The cell survival model derived in this work exhibits exponential cell survival at a high dose and a finite gradient of cell survival at vanishing dose, as well as the dependence on dose-rate.

Keywords Radiation action · Nanodosimetry · Ultra-soft-x-rays · Track-event theory

Introduction

It is generally accepted that the quantity of absorbed dose is not adequate to describe the biological effects of ionizing radiation. The absorbed dose required to produce a given biological effect depends on the radiation quality, which is defined by the type and energy of particles forming a radiation field. Therefore, assessment of the absorbed dose alone is not sufficient when the biological effect of ionizing radiation is of importance, as it is in radiation protection, space radiation research and radiotherapy. Consequently, if the concept of absorbed dose is used the relative biological effectiveness (RBE) of the radiation quality must also be taken into account.

In principle nanodosimetry offers an alternative to time-consuming biological experiments, if the biological effectiveness of ionizing radiation is to be estimated on the basis of physical measurement. It must be noted, however, that such an approach does not consider any chemical and biological interaction. Because nanodosimetric quantities correlate with biological radiation damage, a formulation of radiation action based on nanodosimetric considerations can be viewed as the currently closest physical approach to describe and predict biological effects. In nanodosimetry the stochastic properties of the so-called ionization cluster size, i.e. the number of ionisations produced within a specified basic interaction volume (BIV), typically of the size of the DNA strand, by the interaction of single charged particles, is investigated experimentally or by Monte Carlo simulations. However, it is still not clear which nanodosimetric quantity or which combination of nanodosimetric quantities represent

✉ Uwe Schneider
uwe.schneider@uzh.ch

[1] Department of Physics, Science Faculty, University of Zürich, Zurich, Switzerland

[2] Radiotherapy Hirslanden, Witellikerstrasse 40, 8032 Zurich, Switzerland

the biological effects of ionizing radiation best (Carpenter et al. 2017). It is commonly assumed that the basic damage that might lead to cell death are double strand breaks (DSBs) of the DNA. Therefore, nanodosimetric quantities are defined within nano-sized volumes (Grosswendt et al. 2007). However, there is experimental evidence that several pathways could lead to cell death, each of which interacts on different dimensions from nanometers to micrometers or even larger (Goodhead 2006; Friedrich et al. 2018). As a consequence, any nanodosimetric description will rely on the pattern of lesions and sublesions, which then determines the observed effects. In general, radiation action includes a broad spectrum of such mechanisms, and it is difficult to provide a mathematical formulation which covers all the possible mechanisms such that the nanodistribution of ionisations as well as the geometry of the sensitive structures in the cell is accounted for. Consequently, various simplifications were necessary which may restrict the applicability and the accuracy of the theoretical treatment described below.

In the last few years several radiation action models were developed focusing on biological damage (Carante et al. 2015; Matsuya et al. 2018; McMahon et al. 2016; Wang et al. 2018). Most of these models include several parameters for expressing the biological characteristics of the cell lines, and none of them apply directly to measurable nanodosimetric parameters that could be used to quantify radiation action.

In the following a mathematical description of radiation action is presented, based on nanodosimetric quantities, which is aimed to describe the biological effectiveness of all radiation qualities. The mathematical treatment described below leads to a relatively simple general formula, which is then applied to ultra-soft X-rays. In particular, ultra-soft X-rays were chosen as it is known that microdosimetric approaches, which use micron-sized volumes, are inadequate for describing the biological effects of ultra-soft X-rays. Ultra-soft X-rays produce only low-energy electrons with short ranges (typically < 20 nm), and are a useful probe to study mechanisms of radiation action (Goodhead 2006; Cucinotta et al. 2012; Kellerer et al. 1980). The presented work is based on a previously developed track-event model (Besserer and Schneider 2015a) of cell survival based on simple Poisson statistics. The track event model evolved from a mechanistic description of the involved processes, which are adapted in this work to the current knowledge of biological targets relevant to describe radiation action. As a result, the description of radiation action depends on measurable nanodosimetric quantities, the cell-specific intersection cross-section, and the dose-rate.

Materials and methods

The biological target

An excellent review of the current knowledge on the characteristics of the relevant biological targets, and in particular their sizes and structures in relation to the microscopic features of the radiation, was given by Goodhead (2006). In summary, current evidence suggests typical dimensions in the range of 3–10 nm to be particularly important for initial clustered damage in DNA, primarily responsible for most targeted biological effects in cells. Furthermore, dimensions of 100–500 nm are important for interactions or rearrangements of some of the initial, possibly sublethal damage, ~ 10,000 nm for intracellular and non-targeted effects, and up to millimeters or more for inter-cellular bystander effects and influences on the tissue microenvironment (Goodhead 2006). In the following treatment inter-cellular and non-targeted effects are not considered.

The production of clustered DNA damage in volumes of 3–10 nm in diameter is a characteristic of all radiation qualities, which results in a certain number of complex DSBs (Goodhead 2006). The clustered damage is predominantly confined to small distances along the DNA and is produced almost exclusively within single radiation tracks (Goodhead 2006). The DNA damage on the 100–1000 nm scale involves interactions or rearrangements of some of the initial damage, especially at higher doses and as visualized particularly by chromosome exchanges (Goodhead 2006).

It is assumed here that a sublesion is always a DSB of DNA that is formed in a volume with a diameter of about 2.5 nm including around 10 base pairs, which in the following is called basic interaction volume (BIV). The BIV is synonymous with the nanodosimetric measurement volume described below. Clustered damage is then defined as the accumulation of two or more DSBs in a volume with a diameter of 3–10 nm. The volume in which clustered damage occurs is here called cluster-lesion-volume (or cluster-volume) with a characteristic diameter d_{CV}. Because of the fact that the probability that two independent radiation tracks interact on such small volumes is negligible (Goodhead 1989; Schneider et al. 2017), it is assumed that cluster-lesions (CLs) are always produced by single radiation tracks. On the contrary, pairs of sublesions (SLs) created by one or more radiation tracks can combine to form a distant lesion (DL), as long as the sublesions do not belong to a cluster volume. These DLs can interact with each other over large distances (> 10 nm) and can be created by one or more radiation tracks. Figure 1 shows the combination of SLs to form DLs and CLs.

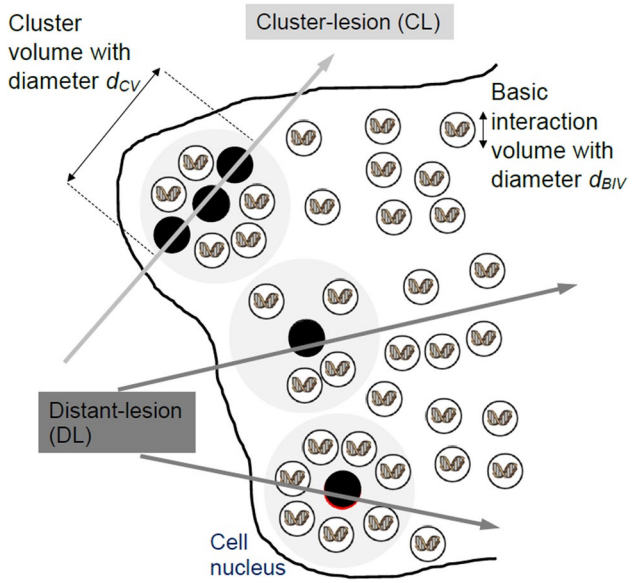

Fig. 1 Arrangement of basic interaction volumes (BIVs) and cluster lesion volumes (CVs) in the cell nucleus. The basic damage (DSB) occurs in the BIV (indicated by a black dot) which is a 10 base-pair section of the DNA strand. An accumulation of DSBs in a larger CV can lead to cluster lesion (CL). Distant sublesions (SLs) can interact to form distant lesions (DLs) (e.g. chromosome aberrations)

Cell survival probability

The radiation action theory presented in the following is based on the track-event model of cell survival, which was developed by applying Poisson statistics to radiation events (Besserer and Schneider 2015a, b). If it is assumed that the formation of one CL or one DL is independent of the formation of other CLs and DLs, respectively, the probabilities for those events can be obtained from Poisson statistics. It is assumed in the model that a cell will survive irradiation if no CL or at most one SL occurs. By taking the first two terms of the Poisson-statistic into account the probability of cell survival is then:

$$S = (e^{-\overline{\mathrm{SL}}} + \overline{\mathrm{SL}} \times e^{-\overline{\mathrm{SL}}}) \times e^{-\overline{\mathrm{CL}}} = \left(1 + \overline{\mathrm{SL}}\right) \times e^{-\overline{\mathrm{SL}}-\overline{\mathrm{CL}}}, \quad (1)$$

where S is the probability for survival and $\overline{\mathrm{CL}}$ is the mean number of cluster lesions. Here it is assumed that CLs and DLs are mutually independent which allows to treat them as independent Poisson distributions. The mean number of sublesions $\overline{\mathrm{SL}}$ is calculated from the number of sublesions which do not contribute to cluster lesions. The mean number of cluster lesions can be expressed as:

$$\overline{\mathrm{CL}} = \phi \times \sigma \times P_{\mathrm{CL}}, \quad (2)$$

where Φ is the particle fluence. The total interaction-cross-section is here factorized into the intersection-cross-section σ and the probability P_{CL} that the particle track interacts. $\Phi{\cdot}\sigma$ is then the probability that a particle track intersects any BIV in the cell nucleus. The probability that the particle track interacts and creates a cluster lesion is given by P_{CL}. It should be noted here that σ contains all cell specific parameters which affect cell sterilization, as e.g. phase in cell cycle, radioresistance, repopulation and repair capability.

The mean number of sublesions is

$$\overline{\mathrm{SL}} = \phi \times \sigma \times \frac{1}{8} \times P_{\mathrm{SL}}, \quad (3)$$

where P_{SL} is the probability that the track interaction creates a sublesion. In Eq. 3 the persistence-parameter 1/8 was included, as it is well known (Dobbs et al. 2008; Antonelli et al. 2015; Pastwa et al. 2001; Reynolds et al. 2012) that the repair of a cluster and simple damage is different, such that sublesions are more efficiently repaired than clustered damage. This persistence-parameter describes the number of unrepaired sublesions relative to the number of unrepaired cluster damage. The persistence-parameter 1/8 in Eq. 3 was determined from experimental evidence as described in Appendix A.

While a DSB is defined in this work as the occurrence of two or more ionisations in a BIV, a cluster lesion consists of the accumulation of a discrete number of n BIVs. If it is assumed that the cluster lesion is of spherical shape with diameter d_{CV}, the mean cord length of a radiation track through a cluster lesion is $2/3{\cdot}d_{\mathrm{CV}}$. As a discrete number of n BIVs forms the cluster lesion the corresponding diameter is given by $d_{\mathrm{CV}} = \frac{3}{2} \times n \times 2.5\mathrm{nm}$. Therefore, the probability to form a cluster event can be calculated using the Binominal distribution, and one gets for the probability for a clustered lesion (two or more BIVs):

$$P_{\mathrm{CL}} = 1 - \left(1 - F_2\right)^n - F_2 \times n \times \left(1 - F_2\right)^{n-1} \quad (4)$$

Here it is assumed that the probability to create a DSB in a BIV is equal to the cumulative nanodosimetric quantity F_2 established by Grosswendt et al. (2007). F_2 is the measurable probability of two or more ionisations which in the context of this work is equivalent to the occurrence of a DSB. It should be noted that d_{CV} must be a multiple of 3.75 nm, since n is an integer.

On the other hand a sublesion (SL) is defined as exactly one DSB inside a volume of diameter d_{CV}. Consequently, the interaction probability P_{SL} for a SL is:

$$P_{\mathrm{SL}} = F_2 \times n \times \left(1 - F_2\right)^{n-1}. \quad (5)$$

Equations (1)–(5) can now be used to calculate survival as a function of the particle fluence, the nanodosimetric quantity F_2 and the cell-specific cross-section σ (Eq. 6):

$$S = \left(1 + \phi \times \sigma \times \frac{1}{8} \times F_2 \times n \times \left(1 - F_2\right)^{n-1}\right) \times e^{-\phi \times \sigma \times \frac{1}{8} \times F_2 \times n \times \left(1-F_2\right)^{n-1} \times (1+\epsilon)}, \quad (6)$$

where it is convenient to define ε as the ratio of complex and simple damage:

$$\varepsilon = \frac{8 \times \left(1 - \left(1 - F_2\right)^n - F_2 \times n \times \left(1 - F_2\right)^{n-1}\right)}{F_2 \times n \times \left(1 - F_2\right)^{n-1}}. \quad (7)$$

Here, simple damage refers to isolated DSBs in a sphere of diameter d_{CV}, while complex damage refers to the accumulation of two or more DSBs in the same volume.

Although a nanodosimetric-based model of radiation action does not rely on dose and RBE, it might be convenient to express Eq. (6) in terms of absorbed dose *D,* to compare any predictions of the presented model with results of cell-survival experiments and RBE measurements. For such a comparison fluence can be expressed in terms of M_1, which is the mean number of ionisations in a BIV and which can be obtained from the nanodosimetric cluster-size distribution:

$$\phi = \frac{D \times \rho \times V}{M_1 \times W_i \times A} = \frac{2 \times D \times \rho \times d_{\mathrm{BIV}}}{3 \times M_1 \times W_i}, \quad (8)$$

where W_i is the mean ionization energy and d_{BIV} and V are the diameter and volume of the basic interaction volume. The area of the two-dimensional projection of the BIV is A. For ultra-soft X-rays $W_i = 25.5$ eV (Schneider et al. 2017) and $\rho = 1$ g/cm^3. Alternatively, one could also calculate the absorbed dose from fluence by using LET instead of M_1. Equation (8) can be used with Eq. (6) to calculate absorbed dose as a function of the survival level and, consequently, RBE can be calculated as the ratio of absorbed dose from a reference radiation to that from the radiation of interest:

$$RBE = \frac{M_1^{\mathrm{ref}} \times \left(1 - F_2^{\mathrm{ref}}\right)^{1-n} \times F_2 \times (1+\epsilon) \times \left\{1 + \epsilon^{\mathrm{ref}} + W\left(-S \times \left(1 + \varepsilon^{\mathrm{ref}}\right) \times e^{-\left(1+\epsilon^{\mathrm{ref}}\right)}\right)\right\}}{M_1 \times \left(1 - F_2\right)^{1-n} \times F_2^{ref} \times \left(1 + \epsilon^{ref}\right) \times \left\{1 + \epsilon + W\left(-S \times (1+\epsilon) \times e^{-(1+\epsilon)}\right)\right\}} \quad (9)$$

where W is the negative branch of the Lambert-function and S the survival level at which RBE is determined. The index "*ref*" labels the reference radiation for which in the following the data of Co-60 γ-rays are used. It should be noted here that RBE in this formulation is independent of the cell-specific parameter σ. The only free parameter in Eq. (9) is the diameter of the cluster volume which is implicitly included in *n.* Thus, a fit of experimental RBE data allows the determination of the cluster volume size. The RBE as defined by Eq. (9) was derived from a more general formulation as compared to that of Schneider et al. (2019) which is somewhat over-simplified.

It can be of interest to evaluate RBE in the limit of high LET or large M_1, respectively. In this case sublethal damage and thus distant lesions are of less importance than clustered damage. Thus, for $\overline{\mathrm{CL}} \gg \overline{\mathrm{SL}}$ Eq. (9) becomes:

$$\mathrm{RBE} = \frac{M_1^{\mathrm{ref}} \times \left(1 - F_2^{\mathrm{ref}}\right)^{1-n} \times \left(1 - F_2 \times \left(1 - F_2\right)^n - n \times F_2 \times \left(1 - F_2\right)^{n-1}\right) \times \left\{1 + \epsilon^{ref} + W\left(-S \times \left(1 + \varepsilon^{ref}\right) \times e^{-\left(1+\epsilon^{ref}\right)}\right)\right\}}{M_1 \times \ln(S) \times n \times F_2^{\mathrm{ref}} \times \left(1 + \epsilon^{\mathrm{ref}}\right)}. \quad (10)$$

Monte Carlo simulation of nanodosimetric quantities

Information on the track-average nanodosimetric quantities, in particular F_2, of electrons generated by photons is important, as those quantities play a fundamental role as a basis for an adequate analysis of radiation effects and damage in matter. When interacting with matter, ultra-soft X-rays release *primary electrons*, which produce low-energy *secondary-electron* cascades along their tracks. Track-average nanodosimetric quantities were obtained here in two steps. First, F_2 was obtained from simulated cluster size distributions in DNA-sized volumes for mono-energetic electrons with energies between 10 eV and 1 MeV (larger electron energies were included as they are used as reference radiation). Second, complete electron tracks of the *primary electrons* were simulated. The resulting track-length distribution was then integrated using the energy-dependent F_2 values yielding the track-averaged F_2. The procedure applied here is similar to that when track-averaged LET values are calculated.

A toolkit for the simulation of the passage of electrons through matter, NOREC (Semenenko et al. 2003) was used for energies between 10 eV and 1 MeV. In the first Monte Carlo simulation, the cluster size distributions were simulated in a spherical BIV of 2.5 nm diameter consisting of water. This BIV size was chosen because it corresponds approximately to a cylindrical DNA volume with 10 base pairs. Electrons were produced at the BIV surface with energy E. The number of ionisations in the BIV was recorded for each particle. For each energy 10^6 electrons

were simulated. Finally, the distribution of ionization clusters was normalized and F_2 and M_1 were computed.

For the simulation of the complete electron tracks of the *primary electrons*, the average energy of the photons transferred to the electrons must be known. The energy of the *primary electrons* was set equal to the photon energy in the energy range where the photoelectric effect is dominant. In the Compton energy range, it was assumed that the electron energy is equal to the photon energy multiplied by the ratio of the energy transfer cross-section and the total cross-section. For the intermediate energy range the average energy of the *primary electrons* was determined by weighting with the photoelectric and Compton cross-section, respectively. Details can be found in Table 1. For each energy in Table 1, 1000 *primary electrons* with all their secondary electrons were simulated. Monte Carlo simulations were performed on a $2\times2\times2$ nm^3 grid. The track length of an electron with certain energy was defined as the straight-line connection between the location of an ionization/excitation were the electron had energy E and the next ionization/excitation where the electron lost energy. Then a frequency distribution of the track length per electron energy (with a resolution of 10 eV) was computed for each track and averaged over the 1000 simulations. The track length distribution was normalized and used to weight the previously determined cluster size distributions of mono-energetic electrons. The resulting integrated cluster size distribution was assumed to represent the distribution of ionisations of a photon beam with a mean energy E. The track-length averaged F_2 is listed in Table 1 for the radiation qualities studied in this work.

Experimentally obtained RBE and cell survival

The predicted RBE values from Eq. 9 were compared to experimentally obtained RBE values of X-rays from the literature, to obtain the size of the cluster volume d_{CV}. For photons, the experimental data collected by Liang et al. (2017) and Buch et al. (2018) were used. The data from Liang et al. (2017) were given as low-dose limiting RBE and, thus, they were compared to values calculated with Eq. 9 by using an arbitrarily chosen $S=0.9$. The data of Buch et al. (2018) were obtained for a survival level of $S=0.1$.

Experimental data of cell survival as a function of dose for ultra-low energy photons were taken from de Lara et al. (2001), Carpenter et al. (2017), Brenner et al. (1987), Botchway et al. (1997) and Raju et al. (1987). De Lara et al. (2001) determined cell survival in Chinese hamster V79-4 cells irradiated as a monolayer with characteristic carbon K-shell (C_K) (0.28 keV), titanium K-shell (Ti_K) (4.55 keV) ultra-soft X-rays and ^{60}Co γ-rays. Carpenter et al. (2017) used CHO-10B cells and determined cell-killing for carbon-K (0.28 keV), aluminum-K (1.5 keV) X rays and ^{60}Co γ-rays. Brenner et al. (1987) determined the inactivation of synchronized V-79 cells by ultra-soft aluminum characteristic X-rays of energy 1.5 keV and ^{137}Cs γ-rays. They measured survival for cells in G_1/S and late S stage. Botchway et al. (1997) used characteristic aluminum K (1.5 keV), copper L (Cu_L) (0.96 keV) ultra-soft X-rays and ^{60}Co γ-rays to investigate cell survival in Chinese hamster V79-4 cells. Finally, Raju et al. (1987) reported on data obtained with cultured hamster cells (V79) exposed to carbon K (0.28 keV), aluminum K (1.5 keV) X rays, copper K (8.0 keV) and 250 kVp X rays.

Table 1 Average energy of *primary electrons* produced by photon irradiation in water

Radiation quality	$\frac{\sigma_{Tr}^{C}}{\sigma^{C}}$	$\frac{\sigma_{C}}{\sigma^{C}+\sigma^{Ph}}$	Average energy of primary electrons [keV]	F_2	M_1
Co-60	0.44	1.000	440	0.00631	0.0341
Cs-137	0.38	1.000	254	0.00825	0.0445
250 kVp	0.22	0.998	69.8	0.0210	0.111
8 keV	1.5E−2	0.014	8.00	0.0631	0.318
4.5 keV	8.7E−3	1.92E−3	4.50	0.0794	0.391
1.5 keV	2.9E−3	1.98E−5	1.50	0.117	0.530
0.96 keV	1.9E−3	3.11E−6	0.96	0.136	0.588
0.28 keV	5.5E−4	9.07E−7	0.28	0.175	0.686

For the photoelectric effect, it was assumed that the electron energy is equal to the photon energy (neglecting binding energy). For the Compton electrons, it was assumed that the energy is equal to the photon energy multiplied by the ratio of the energy transfer σ_{Tr}^{C} and total σ^{C} cross-section (taken from Attix (2004) and listed in column 2). The estimated energies of the photoelectrons and Compton electrons were averaged by weighting them with the energy-dependent ratio of the cross-sections for photoelectric effect σ^{Ph} and Compton scattering σ^{C} (taken from Berger et al. (1998) and listed in column 3). In addition the Monte Carlo simulated values of M_1 and F_2 for the different radiation qualities are listed

Variation of cell survival with dose-rate

It is known that cell survival after photon irradiation changes markedly over a range of dose rates from 0.02 to 0.2 Gy/min, with little further change above or below these dose-rates (Ruiz de Almodóvar et al. 1994). The interpretation of such results has been that low dose-rate repair can occur during irradiation, thus increasing survival. However, such dose-rate sparing is never complete, and this has led to the suggestion that two types of damage are inflicted by ionizing radiation, one which is irreparable (cluster lesions) and another which is repairable (sublesions) (Ruiz de Almodóvar et al. 1994). At high dose-rate sublesions interact to form distant lesions before effective repair can take place. In contrast, at low dose-rate repair of sublesions dominates so that only cluster lesions remain. It was therefore assumed that the dose-rate dependence of repair affects only sublethal damage considered by introducing a factor R which approaches zero for large dose-rates. Consequently, the interaction probability for a SL becomes:

$$P_{\mathrm{SL}} = F_2 \times (1-R) \times n \times \left(1-F_2\right)^{n-1} \tag{11}$$

The radiation action model using Eq. 11 instead of Eq. 5 was fitted to experimental cell survival curves obtained over a large range of dose-rates (Ruiz de Almodóvar et al. 1994; Tonkin et al. 1989; Hall et al. 1986; Sullivan et al. 1996; Steel et al. 1987; Wells and Bedford 1983; DeWeese et al. 1998) to obtain the repair factor R.

Results

Cluster size distributions

The track-average cluster size distributions for the radiation qualities investigated in this work (listed in Table 1) are plotted in Fig. 2. From the track-average cluster size distributions the track-averaged F_2 and M_1 were determined which are also listed in Table 1 and used for further analysis.

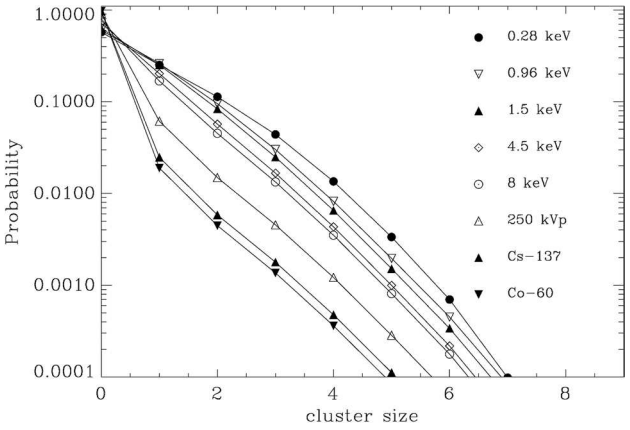

Fig. 2 Track-average cluster size distributions for the radiation qualities as calculated in this work

Determination of cluster volume size

The RBE was computed with Eq. 9 for photons by taking as reference radiation ^{60}Co γ-rays and survival levels S of 0.1 and 0.9. The use of the Binominal distribution for obtaining the interaction probabilities requires integer numbers of n. Thus, the experimental RBE data (Liang et al. 2017; Buch et al. 2018) were fitted to Eq. 9 by using d_{CV}= 3.75, 7.5, 11.25 and 15 nm. It was found that the data fitted best by using 7.5 nm as the diameter for the cluster

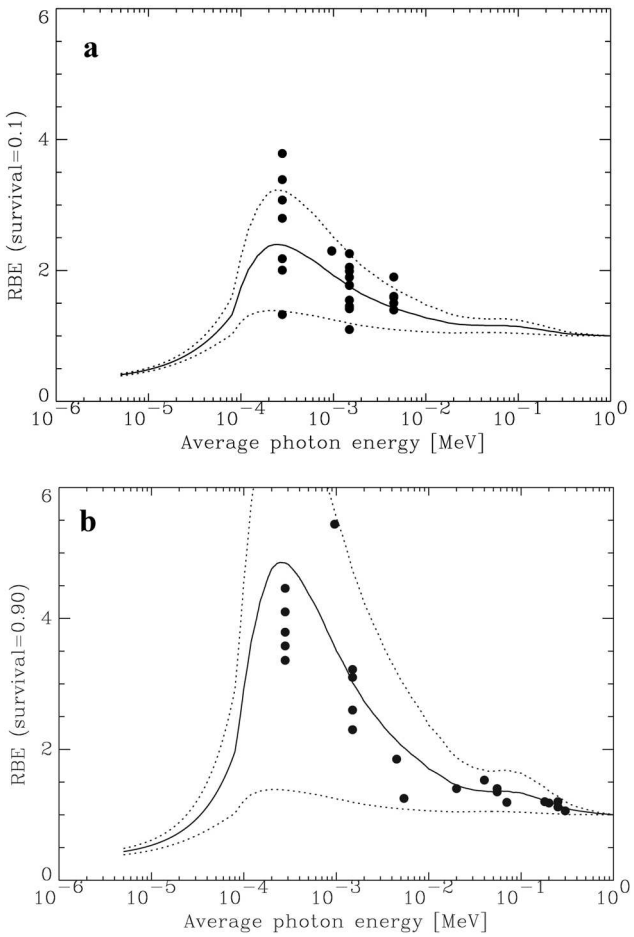

Fig. 3 Calculated photon RBE values (using Eq. 9) as a function of average photon energy (solid lines) for a surviving fraction of 0.1 (**a**) and 0.9 (**b**), respectively. The diameter of the cluster volume (CV) was 7.5 nm (n=2). The symbols represent experimentally obtained RBEs from cell survival measurements taken from Liang et al. (2017) and Buch et al. (2018). Upper and lower dashed lines—calculated RBE for CV diameters of 3.75 nm (n=1) and 11.25 nm (n=3), respectively

volume. The modeled RBE curves with d_{CV} = 7.5 nm are shown in Figs. 3a, b for survival levels of 0.1 and 0.9, respectively. A volume with a diameter of 7.5 nm for cluster damage is in agreement with experimental evidence using ultra-soft X-rays (de Lara et al. 2001; Carpenter et al. 1989; Brenner et al. 1987; Botchway et al. 1997; Raju et al. 1987) and correlated ions (Kellerer et al. 1980). In addition the calculated RBE for CV diameters of 3.75 nm (n = 1) and 11.25 nm (n = 3) are also shown in Fig. 3.

Determination of cell survival curves

The CV size obtained from a comparison of the calculated RBE values with experimental RBE data (d_{CV} = 7.5 nm) was used in the radiation action model (Eq. 6), where cell survival probability is solely a function of one free parameter σ which contains all cell-type-specific parameters. All factors related to radiation quality come directly from nanodosimetry (F_2, M_1). The survival model (Eq. 6) in combination with Eq. 8 was fitted to experimental survival data (de

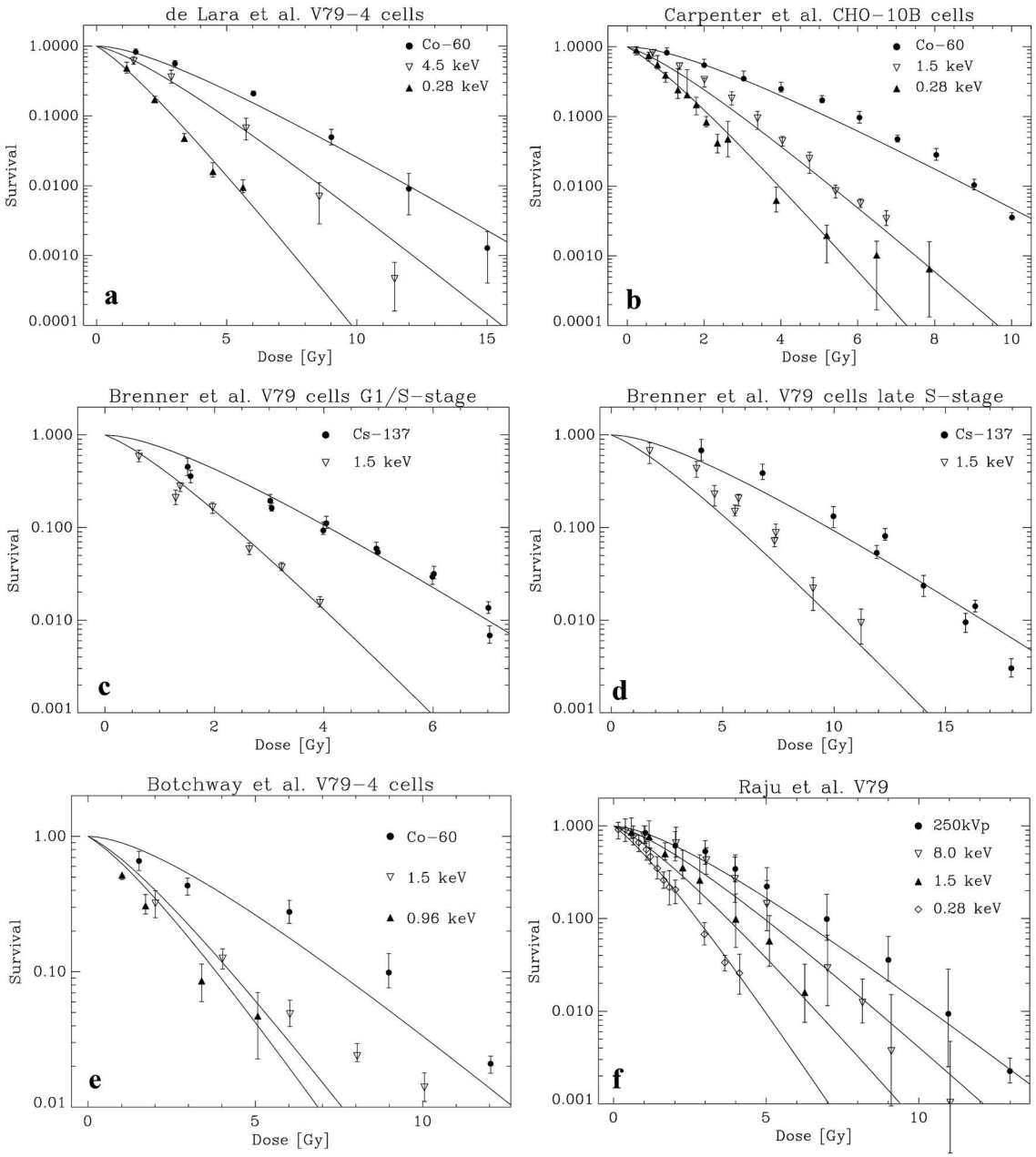

Fig. 4 Modeled cell survival curves for photons of different energies (solid lines). Symbols show experimental data from **a** de Lara et al. (2001), **b** Carpenter et al. (2017), **c**, **d** Brenner et al. (1987), **e** Botchway et al. (1997), and **f** Raju et al. (1987), respectively

Table 2 Results of the model fit to cell survival data

Experimental data	σ/nm^2	d_{CL}/nm	χ^2 of fit	χ^2 of 5% CI
de Lara et al. (2001)	2.87×10^7	6047	17.37*	24.99
Carpenter et al. (2017)	3.87×10^7	7020	20.01*	47.39
Brenner et al. (1987) : G1/S stage	4.88×10^7	7880	14.26*	28.86
Brenner et al. (1987): late S stage	2.05×10^7	5103	23.94*	27.58
Botchway et al. (1997)	2.70×10^7	5866	22.93	22.36
Raju et al. (1987)	3.09×10^7	6273	2.59*	53.38

The first two columns show the fitted parameter in terms of a cross-section σ and diameter d_{CL} of the cluster volume, respectively. The third column lists χ^2 of the fit, while the fourth column shows χ^2 corresponding to the 0.05 confidence level

*Indicates where the model is significant on a 5% level

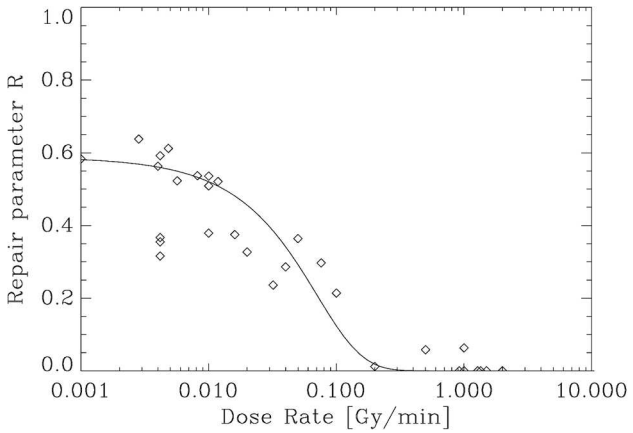

Fig. 5 Repair parameter R (which describes fast repair of sublesions) as a function of dose-rate. Solid line—R obtained from fitting Eq. 12 to experimentally obtained cell survival for photon irradiation at various dose-rates (symbols) (Ruiz de Almodóvar et al. 1994; Tonkin et al. 1989; Hall et al. 1986; Sullivan et al. 1996; Steel et al. 1987; Wells and Bedford 1983; DeWeese et al. 1998)

Lara et al. 2001; Carpenter et al. 1989; Brenner et al. 1987; Botchway et al. 1997; Raju et al. 1987). A least-square fit to all photon energies combined yielded the intersection cross-sections of 2.87×10^7 nm^2, 3.87×10^7 nm^2, 4.88×10^7 nm^2, 2.05×10^7 nm^2, 2.70×10^7 nm^2 and 3.09×10^7 nm^2 for the data from de Lara et al. (2001), Carpenter et al. (1989), Brenner et al. (G1/S stage and late S stage) (1987), Botchway et al. (1997) and Raju et al. (1987), respectively. These cross-sections correspond to equivalent circular intersection cross-sections with diameters 6047 nm, 7020 nm, 7880 nm, 5103 nm, 5866 nm, and 6273 nm, respectively. The corresponding fitted cell survival curves are shown in Fig. 4. Table 2 lists the fitted parameters together with the χ^2 values of the fits. It is noted that all fits except for that to the Botchway data are significant on the 5% level. It should be emphasized here that only the cell-parameter σ was fitted and that the energy dependence of the modeled cell survival is explained exclusively by the energy dependence of F_2 and M_1.

Dose-rate effect

In Fig. 5 the fitted repair parameter R is plotted as a function of dose-rate. An appropriate mathematical description is the logistic function which was fitted to the data shown as the solid line:

$$R = \frac{1}{0.7 + e^{20\times DR}}, \tag{12}$$

where DR is the dose-rate in Gy/min. Some examples of experimental cell survival curves obtained with different dose-rates are shown in Fig. 6 together with predicted curves calculated based on Eq. 12.

Discussion

The theory of radiation action presented in this work was motivated by the finding that the biological effects of various types of ionizing radiation lack a consistent relation on absorbed dose. In the present work it is postulated that the common fundamental cause of these effects is the production of elementary sublesions (DSBs) which are created at a frequency of occurrence that is proportional to the probability to produce more than two ionisations within regions termed basic interaction volumes. The concepts of nanodosimetry permit a quantitative characterization of this process in terms of the cumulative probability F_2. These sublesions can interact in two ways to produce lethal damage. If two or more sublesions accumulate in a locally limited volume with a diameter in the range of 3–10 nm, then clustered DNA damage is produced. Clustered damage is difficult to repair, and is primarily responsible for most conventional targeted effects in cells (Goodhead 2006). Consequent interactions

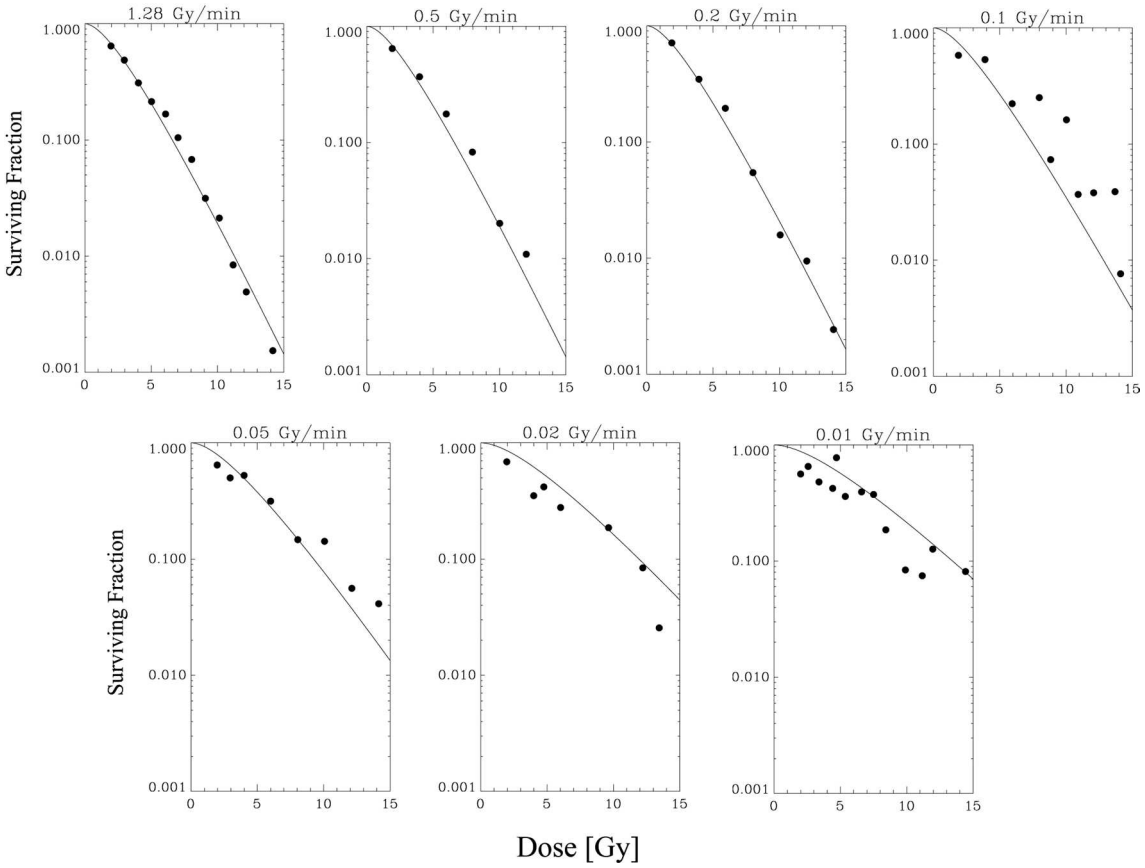

Fig. 6 Plot of the experimentally obtained cell survival data from Ruiz de Almodóvar et al. (1994) as the symbols for dose-rates from 0.01 to 1.28 Gy/min. The solid lines represent model calculations using Eqs. 1, 3, 11 and 12

or rearrangements of some of the initial damage over larger distances (~ µm) can produce also lethal damage, here called distant lesions, which is visualized e.g. by chromosome exchanges (Goodhead 2006).

From the comparison of theoretical with experimental RBE data, a cluster volume with a diameter of 7.5 nm was obtained in the present study. This included only two basic interaction volumes. This finding is in agreement with other experimental evidence, like the biological effectiveness of ultra-soft X-rays data (de Lara et al. 2001; Carpenter et al. 1989; Brenner et al. 1987; Botchway et al. 1997; Raju et al. 1987) and the results of correlated ion experiments (Kellerer et al. 1980; Bird 1997).

In contrast to RBE, cell survival depends in addition on the intersection cross-section which includes all cell-specific factors affecting cell survival. Thus, the modeled cell survival curve has only one free fit parameter. Using ultra-soft X-rays it could be shown that the energy dependence of cell survival is governed directly by the nanodosimetric characteristics of the radiation track structure. The cell survival model derived in this work exhibits exponential cell survival at a high dose and a finite gradient of cell survival at a vanishing dose, which reflects experimental evidence in particular at high dose.

The presented treatment of distant lesions formed by sublesions is similar to that described in the dual radiation action theory of Kellerer and Rossi (1978). Therefore, a lot of limitations of the dual radiation action theory apply also to the present approach, and the discussion is similar to that offered by Kellerer and Rossi (1978). It should be noted, however, that the integration of nanodosimetry into a radiation action model allows a simple treatment of cluster damage, in contrast to the dual radiation action model.

In its current form, the theory presented here is based on various simplifications, the most conspicuous of which being the somewhat arbitrary assumption of spherical sensitive regions in the cell nucleus. The number and the spatial distribution of such sites in the nucleus of the cell have been left unspecified. In fact, the notion of spherical sensitive sites within the nucleus serves merely as an approximation. In nanodosimetry usually cylindrical volumes are used to represent the DNA strand. To allow for the benefits of spherical symmetry, spherical interaction volumes were used here. In terms of the determination of cluster size distributions,

spherical volumes are not markedly different from cylindrical volumes (Schmidli 2018).

Moreover, it is hypothesized here that sublesions which do not belong to a cluster site have a fixed probability of interacting pairwise. A more realistic assumption might be that the interaction probability of two sublesions depends somehow on the distance between them and, consequently, might be decreasing with increasing distance.

A major limitation of the model framework developed in the present study is that it applies only to cell inactivation. It might well be that a target theory which does not only include cell death but also local effects like transformations or mutations produces different results as compared to those obtained in the present study because it is known that there are various types of lesions (or combinations of lesions) responsible for biological effects observed in cells and tissues. As a consequence, this fact could result in mutual interferences between sublesions which would in turn reduce the frequency of lesions resulting in any specific effect. While this is of considerable importance, it was not included in the formulation presented here.

Another related limitation of the model is that it disregards complications that can arise when the probability for a distant lesion produced by any pair of sublesions is influenced by the presence of a cluster lesion and vice versa. In such circumstances the present model framework produces reasonable results only when the probabilities to form cluster lesions and distant lesions are low, such that they can be regarded as mutually independent.

Another limitation of the present model is that the finite width of the radiation tracks is not considered. A radiation track is assumed here to be as narrow as the width of a basic interaction volume. Another simplification is that the particle trajectories are described as multiples of straight segments with a length of 7.5 nm. Note that, in particular for low-energy electrons, the mean chord length of the electrons through the cluster volume can be smaller than the straight-line approximation.

Furthermore, another limitation of the model is that a realistic spatial arrangement of DNA in the cell nucleus is not considered (Kellerer and Rossi 1978; Schneider et al. 2016). In fact it is assumed that in case a radiation track intersects a BIV and produces a DSB somewhere in the cell nucleus, this DSB is embedded in a volume with a diameter of 7.5 nm that is homogeneously filled by DNA.

The diffusion of primary radiation products such as free radicals is also disregarded in the present model, to reduce its mathematical complexity. Instead, it is simply assumed that each sublesion is formed in a basic interaction volume at the location of any ionization.

Conclusion

In the present paper a model was established that allows the description of biological effects based on nanodosimetric interactions of ionizing radiation, in particular electrons, within cell volumes. With the assumption of a cluster volume with a diameter of 7.5 nm, the model allowed to reproduce experimental RBE values and cell survival curves for photons in the energy range between about 0.28 keV and 1 MeV reasonably well. The presented model should be viewed as a first step to combine nanodosimetry with radiation action models. It can be regarded as starting point for still more generalized models. A report with the application of the presented theory to ions is in progress.

Author contributions US designed this study, performed parts of the simulations and calculations and drafted the manuscript. FV and KS performed parts of the simulations and JB developed the idea for the track event model. All authors read and approved the final manuscript.

Compliance with ethical standards

Conflict of interest The authors report no conflicts of interest.

Appendix A: quantification of the repair of cluster (CL) and simple (SL) lesions

It is well known that complex, clustered DNA damage is less efficiently repaired than simple damage (Dobbs et al. 2008; Antonelli et al. 2015; Pastwa et al. 2001; Reynolds et al. 2012). It has been proposed that the fast component of DSB repair acts predominantly on simple DSBs whereas the slower component of DSB repair acts on DSBs with more complex structures (Reynolds et al. 2012). For the radiation action model developed in the present study it is sufficient to consider the relative rates of DSB rejoining (complex to simple), because the basic cell-specific repair capability is included in the intersection cross-section σ. Pastwa et al. (2001) found a 6-fold lower repair rate for complex damage when compared to simple DNA damage. Antonelli et al. (2015) studied the repair of DNA DSBs for radiation qualities of different LET. In the present study, their measured persistence ratio of DSBs after 4 and 24 h was used, to determine the persistence-parameter for the present model. For this purpose the mean number of cluster lesions and sublesions was calculated for the four radiation qualities used by Antonelli et al. (2015): Cs-137 γ-rays, 28.5 keV/µm protons, 39.4 keV/µm carbon ions and 125 keV/µm α-particles. The persistence ratio PR was then calculated (Eq. 13):

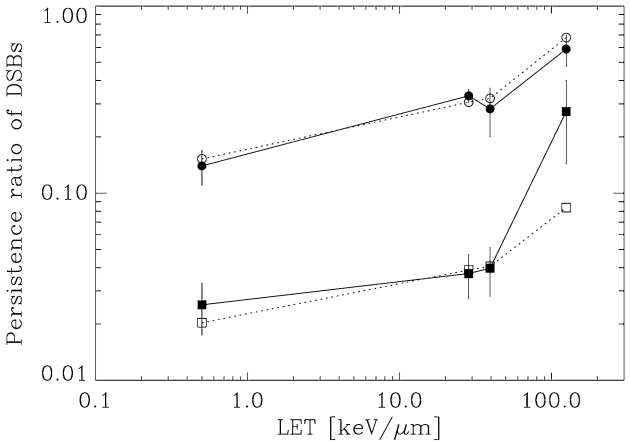

Fig. 7 Persistence ratio of double-strand breaks (DSBs) after irradiation as a function of LET for 4 (circles) and 24 h (squares) after irradiation. Closed symbols represent experimental data (Antonelli et al. 2015), open symbols represent a fit to the experimental data resulting in a persistence-parameter of 0.21 and 0.22 for 4 and 24 h, respectively. The errors were reconstructed from the raw data (Fig. 1 from Antonelli et al. 2015)

Table 3 Experimentally obtained relative rates of DSB rejoining (complex to simple) as described in Appendix A

Experimental data	Relative repair simple/complex
Pastwa et al. (2001)	0.17
Antonelli et al. (2015): 4 h	0.21
Antonelli et al. (2015): 24 h	0.22
de Lara et al. (2001)	0.11
Carpenter et al. (2017)	0.11
Brenner et al. (1987): G1/S stage	0.12
Brenner et al. (1987): late S stage	0.22
Botchway et al. (1997)	0.10

$$\mathrm{PR} = \frac{\mathrm{PR_{CL}} \times \overline{CL} + \mathrm{PR_{SL}} \times \overline{\mathrm{SL}}}{\overline{\mathrm{CL}} + \overline{\mathrm{SL}}} = \frac{\mathrm{PR_{CL}} \times P_{\mathrm{CL}} + \mathrm{PR_{SL}} \times P_{\mathrm{SL}}}{P_{\mathrm{CL}} + P_{\mathrm{SL}}} \tag{13}$$

The parameters $\mathrm{PR_{CL}}$ and $\mathrm{PR_{SL}}$ were then fitted to the experimental *PR*-data from Antonelli et al. (2015) using $n = 2$ and P_{CL} and P_{SL} from Eqs. 4 and 5, respectively. The results of the least square fit are shown in Fig. 7 where the closed symbols represent experimental data and the open symbols the fit. The obtained $\mathrm{PR_{SL}}/\mathrm{PR_{CL}}$ is 0.21 and 0.22 for 4 and 24 h after irradiation, respectively.

In addition the experimental cell survival data (de Lara et al. 2001; Carpenter et al. 1989; Brenner et al. 1987; Botchway et al. 1997; Raju et al. 1987) used in the present work were fitted to the model described by Eq. 6 including the relative repair rate of complex to simple damage as a second fit parameter besides σ. The resulting relative repair rates $\mathrm{PR_{SL}}/\mathrm{PR_{CL}}$ are listed in Table 3 and are in satisfying agreement with other experimental evidence. For the model the relative repair rate was arbitrarily fixed to 1/8.

References

Antonelli F, Campa A, Esposito G, Giardullo P, Belli M, Dini V, Meschini S, Simone G, Sorrentino E, Gerardi S, Cirrone GA, Tabocchini MA (2015) Induction and repair of DNA DSB as revealed by H2AX phosphorylation foci in human fibroblasts exposed to low- and high-LET radiation: relationship with early and delayed reproductive cell death. Radiat Res 183(4):417–431

Attix FH (2004) Introduction to radiological physics and radiation dosimetry. WILEY-VCH, Weinheim

Berger MJ, Hubbell JH, Seltzer SM, Chang J, Coursey JS, Sukumar R, Zucker DS, Olsen K (1998) NIST Standard Reference Database 8: XCOM: photon cross sections database. https://www.nist.gov/pml/xcom-photon-cross-sections-database. Accessed 29 Nov 2019

Besserer J, Schneider U (2015a) A track-event theory of cell survival. Z Med Phys 25(2):168–175

Besserer J, Schneider U (2015b) Track-event theory of cell survival with second-order repair. Radiat Environ Biophys 54(2):167–174

Bird RP (1997) Biophysical studies with spatially correlated ions. 3. Cell survival studies using diatomic deuterium. Radiat Res 78(2):210–223

Botchway SW, Stevens DL, Hill MA, Jenner TJ, O'Neill P (1997) Induction and rejoining of DNA double-strand breaks in Chinese hamster V79-4 cells irradiated with characteristic aluminum K and copper L ultrasoft X rays. Radiat Res 148(4):317–324

Brenner DJ, Bird RP, Zaider M, Goldhagen P, Kliauga PJ, Rossi HH (1987) Inactivation of synchronized mammalian cells with low-energy X rays–results and significance. Radiat Res 110(3):413–427

Buch T, Scifoni E, Krämer M, Durante M, Scholz M, Friedrich T (2018) Modeling radiation Effects of ultrasoft X-rays on the basis of amorphous track structure. Radiat Res 189(1):32–43

Carante MP, Altieri S, Bortolussi S, Postuma I, Protti N, Ballarini F (2015) Modeling radiation-induced cell death: role of different levels of DNA damage clustering. Radiat Environ Biophys 54(3):305–316

Carpenter S, Cornforth MN, Harvey WF, Raju MR, Schillaci ME, Wilder ME, Conte V, Selva A, Colautti P, Hilgers G, Rabus H (2017) Track structure characterization and its link to radiobiology. Radiat Meas 106:506–511

Carpenter S, Cornforth MN, Harvey WF, Raju MR, Schillaci ME, Wilder ME, Goodhead DT (1989) Radiobiology of ultrasoft X rays. IV. Flat and round-shaped hamster cells (CHO-10B, HS-23). Radiat Res 119(3):523–33

Cucinotta FA, Kim MY, Chappell L (2012) Space radiation cancer risk projections and uncertainties-2012. NASA TP 2013:217375

de Lara CM, Hill MA, Jenner T, Papworth D, O'Neill P (2001) Dependence of the yield of DNA double-strand breaks in Chinese hamster V79-4 cells on the photon energy of ultrasoft X rays. Radiat Res 155(3):440–448

DeWeese TL, Shipman JM, Dillehay LE, Nelson WG (1998) Sensitivity of human prostatic carcinoma cell lines to low dose rate radiation exposure. J Urol 159(2):591–598

Dobbs TA, Palmer P, Maniou Z, Lomax ME, O'Neill P (2008) Interplay of two major repair pathways in the processing of complex double-strand DNA breaks. DNA Repair 7(8):1372–1383

Friedrich T, Ilicic K, Greubel C, Girst S, Reindl J, Sammer M, Schwarz B, Siebenwirth C, Walsh DWM, Schmid TE, Scholz M, Dollinger G (2018) DNA damage interactions on both nanometer and micrometer scale determine overall cellular damage. Sci Rep 8(1):16063

Goodhead DT (1989) The initial physical damage produced by ionizing radiations. Int J Radiat Biol 56(5):623–634

Goodhead DT (2006) Energy deposition stochastics and track structure: what about the target? Radiat Prot Dosim 122(1–4):3–15

Grosswendt B, Pszona S, Bantsar A (2007) New descriptors of radiation quality based on nanodosimetry, a first approach. Radiat Prot Dosim 126(1–4):432–444

Hall EJ, Marchese MJ, Astor MB, Morse T (1986) Response of cells of human origin, normal and malignant, to acute and low dose rate irradiation. Int J Radiat Oncol Biol Phys 12(4):655–659

Kellerer AM, Rossi HH (1978) A generalized formulation of dual radiation action. Radiat Res 75(3):471–488

Kellerer AM, Lam YM, Rossi HH (1980) Biophysical studies with spatially correlated ions. 4. Analysis of cell survival data for diatomic deuterium. Radiat Res 83(3):511–528

Liang Y, Fu Q, Wang X, Liu F, Yang G, Luo C, Ouyang Q, Wang Y (2017) Relative biological effectiveness for photons: implication of complex DNA double-strand breaks as critical lesions. Phys Med Biol 62(6):2153–2175

Matsuya Y, Sasaki K, Yoshii Y, Okuyama G, Date H (2018) Integrated modelling of cell responses after irradiation for DNA-targeted effects and non-targeted effects. Sci Rep 8(1):4849

McMahon SJ, Schuemann J, Paganetti H, Prise KM (2016) Mechanistic modelling of DNA repair and cellular survival following radiation-induced DNA damage. Sci Rep 14(6):33290

Pastwa E, Neumann RD, Winters TA (2001) In vitro repair of complex unligatable oxidatively induced DNA double-strand breaks by human cell extracts. Nucleic Acids Res 29(16):E78

Raju MR, Carpenter SG, Chmielewski JJ, Schillaci ME, Wilder ME, Freyer JP, Johnson NF, Schor PL, Sebring RJ, Goodhead DT (1987) Radiobiology of ultrasoft X rays. I. Cultured hamster cells (V79). Radiat Res 110(3):396–412

Reynolds P, Anderson JA, Harper JV, Hill MA, Botchway SW, Parker AW, O'Neill P (2012) The dynamics of Ku70/80 and DNA-PKcs at DSBs induced by ionizing radiation is dependent on the complexity of damage. Nucleic Acids Res 40(21):10821–10831

Ruiz de Almodóvar JM, Bush C, Peacock JH, Steel GG, Whitaker SJ, McMillan TJ (1994) Dose-rate effect for DNA damage induced by ionizing radiation in human tumor cells. Radiat Res 138(1 Suppl):S93–S96

Schmidli K (2018) Monte Carlo simulations of cluster size distributions of various radiation qualities and application to track-event theory and treatment planning. Master thesis of the University of Zurich. https://opac.nebis.ch. Accessed 4 Apr 2018

Schneider U, Vasi F, Besserer J (2016) The impact of the geometrical structure of the DNA on parameters of the track-event theory for radiation induced cell kill. PLoS One. 11(10):e0164929

Schneider U, Vasi F, Besserer J (2017) The probabilities of one- and multi-track events for modeling radiation-induced cell kill. Radiat Environ Biophys 56(3):249–254

Schneider U, Vasi F, Schmidli K, Besserer J (2019) Track event theory: a cell survival and RBE model consistent with nanodosimetry. Radiat Prot Dosim 183(1–2):17–21

Semenenko VA, Turner JE, Borak TB (2003) NOREC, a Monte Carlo code for simulating electron tracks in liquid water. Radiat Environ Biophys 42(3):213–217

Steel GG, Deacon JM, Duchesne GM, Horwich A, Kelland LR, Peacock JH (1987) The dose-rate effect in human tumour cells. Radiother Oncol 9(4):299–310

Sullivan FJ, Carmichael J, Glatstein E, Mitchell JB (1996) Radiation biology of lung cancer. J Cell Biochem Suppl 24:152–159

Tonkin KS, Kelland LR, Steel GG (1989) A comparison of the in vivo and in vitro radiation response of three human cervix carcinomas. Radiother Oncol 16(1):55–56 **(Erratum (1989) Radiother Oncol 16(2))**

Wang W, Li C, Qiu R, Chen Y, Wu Z, Zhang H, Li J (2018) Modelling of cellular survival following radiation-induced DNA double-strand breaks. Sci Rep 8(1):16202

Wells RL, Bedford JS (1983) Dose-rate effects in mammalian cells. IV. Repairable and nonrepairable damage in noncycling C3H 10T 1/2 cells. Radiat Res 94(1):105–134